Energy Materials

Supplementary Materials

Efficient and stable lithium storage of porous carbon fiber composite bimetallic sulfides (FeS-ZnS) anode

Wei Wang[1], Huichuan Tang[1], Joao Cunha[2], Maryam Karimi[2], Najeeb Lashari[2], Aqrab Ahmad[2], Hong Yin[1,2,*]

[1]Key Laboratory of Hunan Province for Advanced Carbon-Based Functional Materials, School of Chemistry and Chemical Engineering, Hunan Institute of Science and Technology, Yueyang 414006, Hunan, China.
[2]International Iberian Nanotechnology Laboratory (INL), Av. Mestre Jose Veiga, Braga 4715-330, Portugal.

***Correspondence to:** Dr. Hong Yin, Key Laboratory of Hunan Province for Advanced Carbon-Based Functional Materials, School of Chemistry and Chemical Engineering, Hunan Institute of Science and Technology, No. 439, Xiangbei Road, Yueyanglou District, Yueyang 414006, Hunan, China. E-mail: hong.yin@inl.int

S1. Material characterization

X-ray diffraction (XRD) was measured using a Rigaku Ultima IV instrument from Japan, equipped with Cu-Kα radiation. Thermogravimetric analysis (TGA) was conducted employing a simultaneous DSC-TGA analyzer (Rigaku TG/DTA8122, Japan) in the temperature range of 30-800 ℃ at a heating rate of 10 ℃ min^{-1} under an air atmosphere. Raman spectra were recorded with a WITec CRM200 instrument utilizing a 532 nm laser. The BET specific surface area was determined using a N_2 adsorption/desorption analyzer (Micromeritics, ASAP 2020 HD), followed by the application of the Barrett-Joyner-Halenda (BJH) method to calculate pore volume. The morphologies of the samples were characterized by field-emission scanning electron microscopy (FE-SEM, JEOL JSM-6330f) and transmission electron microscopy (TEM). TEM analysis was performed on a JEOL JEM-2100 microscope operating at an acceleration voltage of 200 kV. X-ray photoelectron spectroscopy (XPS) analysis was conducted using an AXIS-ULTRADLD-

600W instrument.

S2. Electrochemical measurements

A standard two-electrode coin cell (LIR 2025) was assembled for electrochemical measurements. The active material slurry were prepared by mixing 80 mg of active material, 10 mg of acetylene black, and 10 mg of polyvinylidene difluoride (PVDF) in 0.5 mL of NMP. The resulting slurry was uniformly coated onto copper foil and dried under vacuum at 60 ℃ for 12 hours to prepare working electrodes, with a mass loading of the active material of approximately 1.0 mg cm^{-2}. The electrolyte consisted of 1 mol L^{-1} $LiPF_6$ with dimethyl carbonate, ethylene carbonate, and ethyl methyl carbonate as a mixed solvent (volume ratio of 1:1:1). Celgard 2500 was used as the separator, and lithium foil was used as the counter electrode. Cell assembly took place in a glovebox with an argon atmosphere (water and oxygen contents below 0.1 ppm). Cyclic voltammetry (CV) was performed using an electrochemical workstation (CHI760E) over a voltage range of 0.005-3.0 V (vs. Li/Li^+) at a scan rate of 0.2-1.0 mV s^{-1}. Galvanostatic charge/discharge measurements were carried out on a cell test system (Land CT2001A) within the voltage range of 0.005-3.0 V at room temperature. Electrochemical impedance spectroscopy (EIS) tests were performed in the frequency range of 0.01-100 kHz.

S3. Process dynamics

Determine the apparent Li^+ diffusion coefficient of the corresponding electrode according to Fick's second law calculation (D).

$$D_{Li^+} = \frac{4L^2}{\pi\tau}\left(\frac{\Delta Es}{\Delta Et}\right) \quad \textbf{(S1)}$$

where L is Li^+ diffusion length (cm, it is equal to thickness of electrode for compact electrode); τ is the relaxation time of rest intervals (s); ΔE_s is the steady-state potential difference (V) between two adjacent discharge relaxations, while ΔE_t is the potential difference (V) caused by the constant current pulse after eliminating the iR drop.

S4. Computational details

The density of states (DOS) and electron density difference of FeS-ZnS/PCFs and ZnS/PCFs were calculated by using quantum chemical calculation method based on the density functional theory (DFT) of CASTEP module (Materials Studio 8.0, BIOVIA, San Diego, US). The generalized gradient approximation (GGA) method with Perdew-Burke-Ernzerhof (PBE) functional for the exchange-correlation term was used. A plane-wave basis set with an energy cutoff of 300 eV and 2×2×1 k-point sampling was used for Brillouin zone (BZ). The electronic and ionic convergence criteria were respectively set to 10^{-5} eV and 0.03 eV·Å^{-1}, and all calculations were performed spin-polarized. In the calculations, geometry optimization of all the atoms in the structure were performed.

The *d* band center (ε_d) of transition metal atom is calculated by following equation:

$$\varepsilon_d = \int_{-\infty}^{\infty} x\rho(x)dx \Big/ \int_{-\infty}^{\infty} \rho(x)dx \quad \text{(S2)}$$

where the $\rho(x)$ refers to the d-typed PDOS of the corresponding transition metal atom.

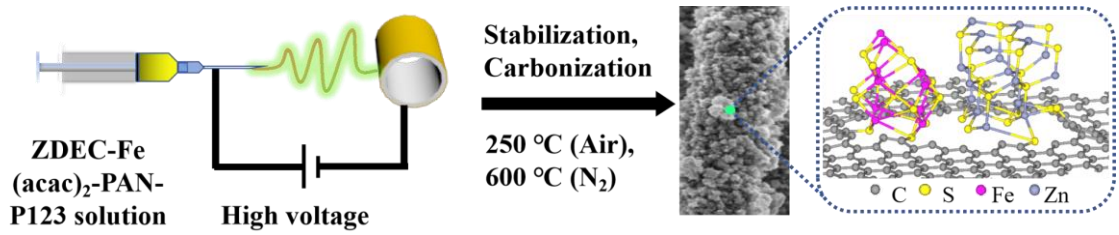

Supplementary Figure 1. Representation of the synthesis of FeS-ZnS/PCFs.

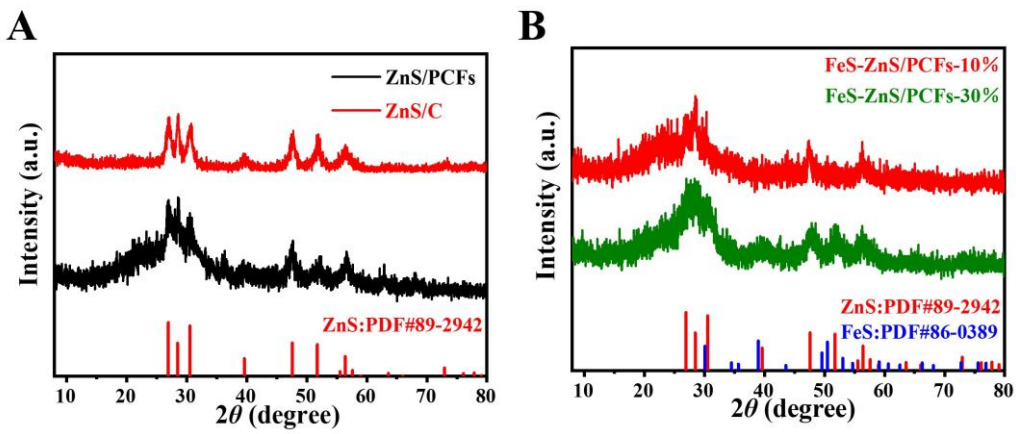

Supplementary Figure 2. A: XRD patterns of ZnS/PCFs and ZnS/C; B: FeS-ZnS/PCFs-10% and FeS-ZnS/PCFs-30%.

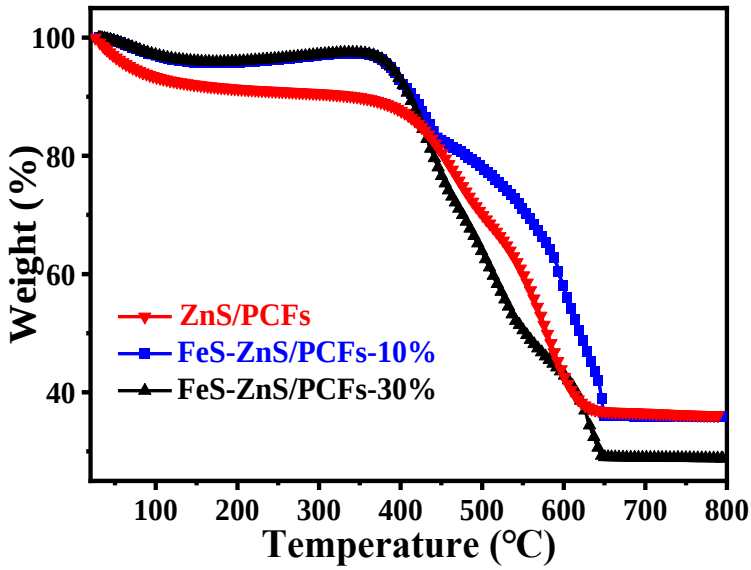

Supplementary Figure 3. TG curves of ZnS/PCFs, FeS-ZnS/PCFs-10% and FeS-ZnS/PCFs-30%.

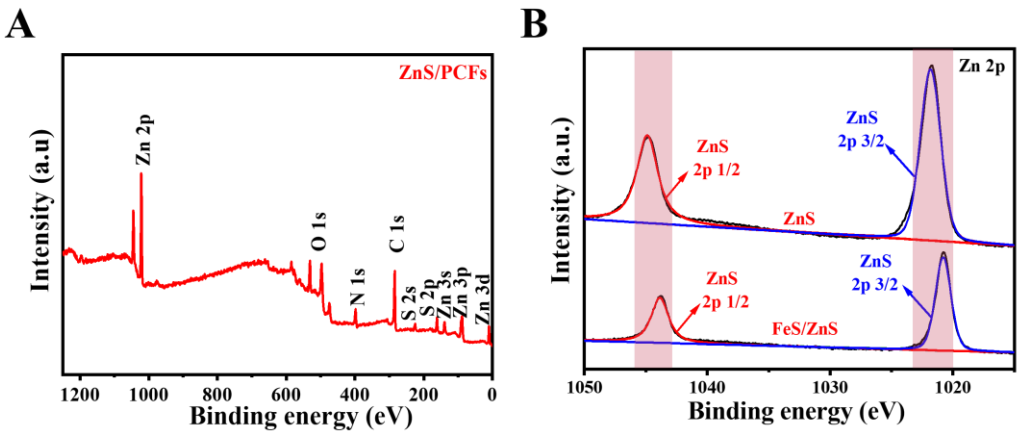

Supplementary Figure 4. A: XPS survey spectra of the ZnS/PCFs; B: High-resolution Zn 2p spectra of ZnS/PCFs and FeS-ZnS/PCFs-20%.

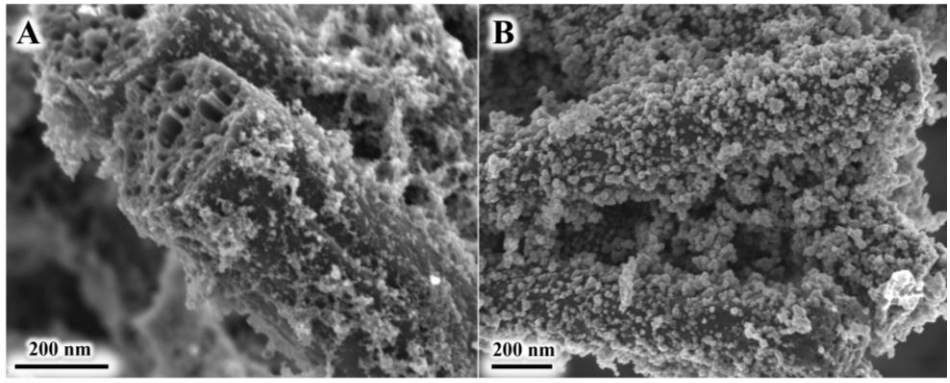

Supplementary Figure 5. A**:** SEM images of FeS-ZnS/PCFs-10%; B: SEM images of FeS-ZnS/PCFs-30% (B).

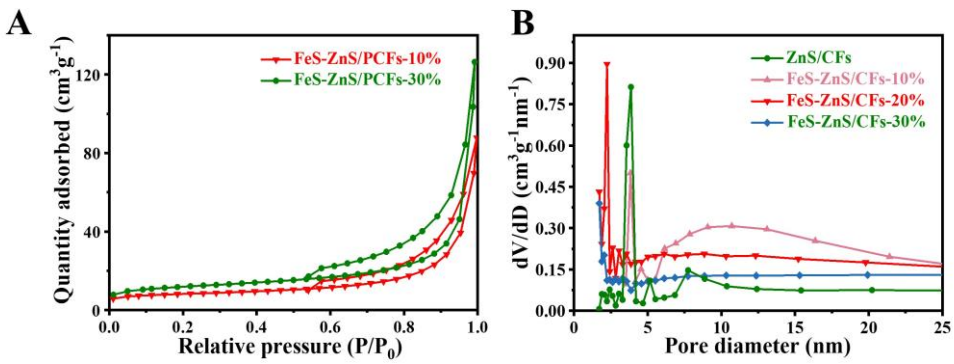

Supplementary Figure 6. A: N_2 adsorption-desorption isotherms; B: BJH pore-size distribution of samples

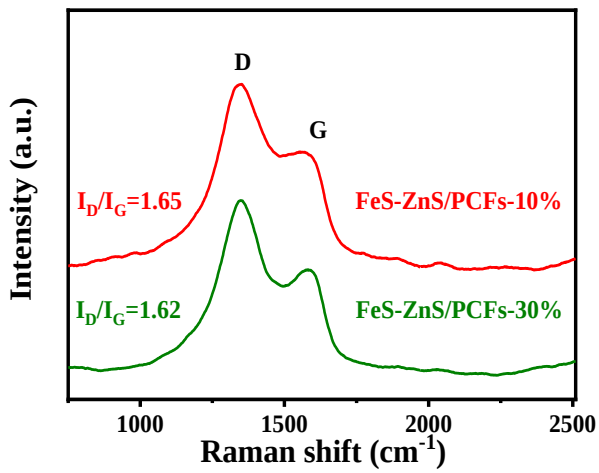

Supplementary Figure 7. Raman spectra of FeS-ZnS/PCFs-10% and FeS-ZnS/PCFs-30%.

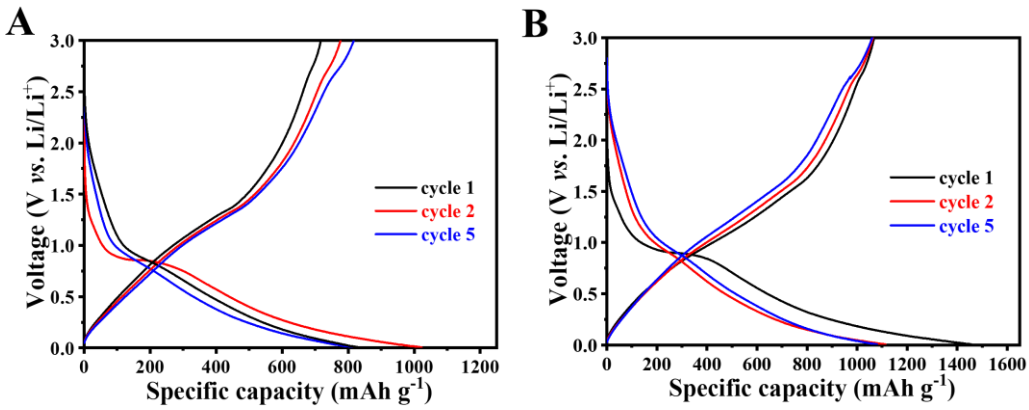

Supplementary Figure 8. A: 1st, 2nd, 5th GCD profiles of the FeS-ZnS/PCFs-10% anode at 0.2 A g^{-1}; B: 1st, 2nd, 5th GCD profiles of the FeS-ZnS/PCFs-30% anode at 0.2 A g^{-1}.

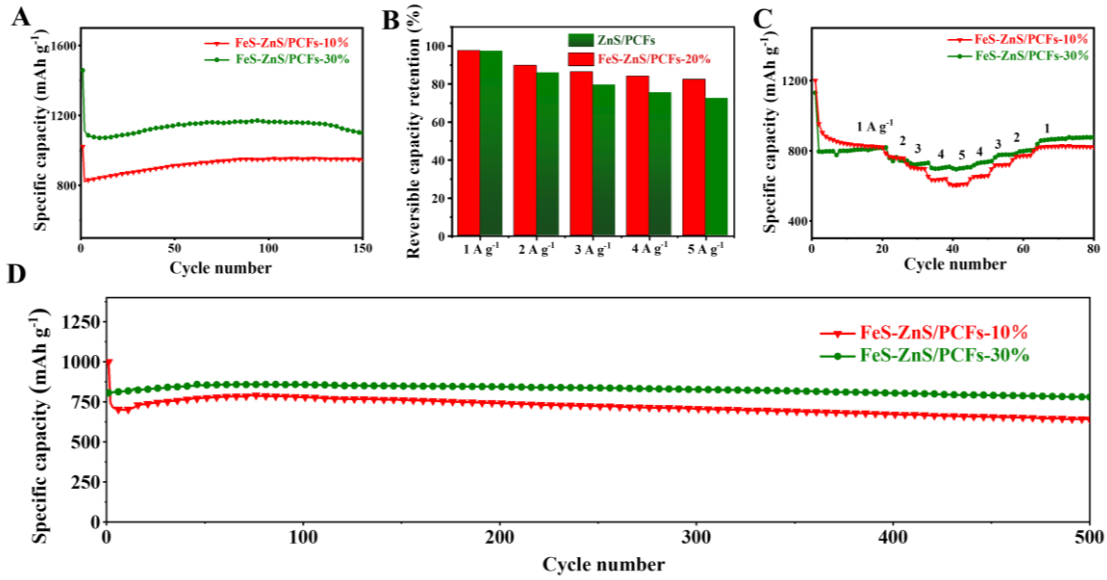

Supplementary Figure 9. A: Cycling performance of the FeS-ZnS/PCFs-10% and FeS-ZnS/PCFs-30% anodes at 0.2 A g^{-1}; B: Rate performance of the ZnS/PCFs and FeS-ZnS/PCFs-20% anodes at different current densities of 1 A g^{-1}, 2 A g^{-1}, 3 A g^{-1}, 4 A g^{-1} and 5 A g^{-1}; C: Histogram of capacity retention at different current densities; D: Long cycling performance of the FeS-ZnS/PCFs-10% and FeS-ZnS/PCFs-30% anodes at current density of 1 A g^{-1}.

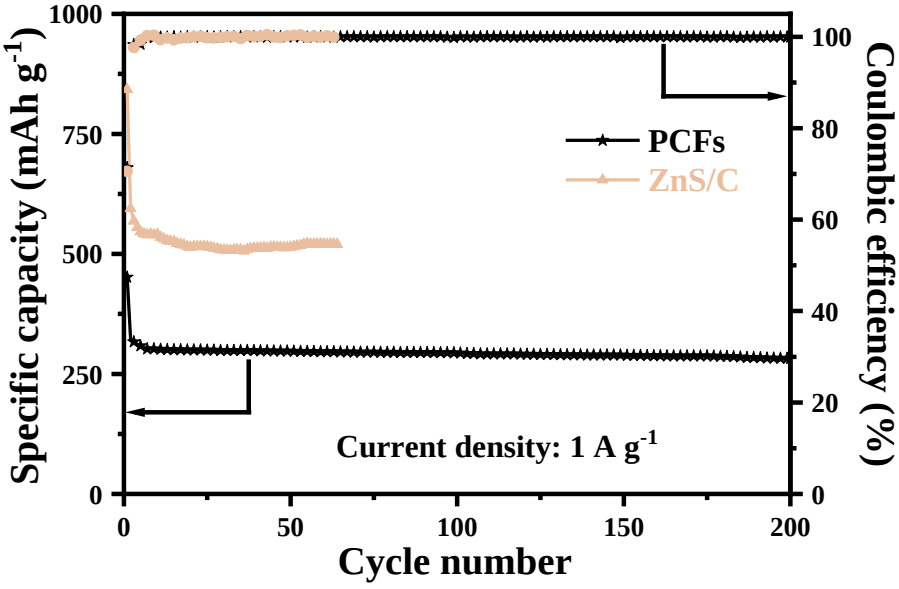

Supplementary Figure 10. Long cycling performance of the PCFs and ZnS/C anodes at current density of 1 A g^{-1}.

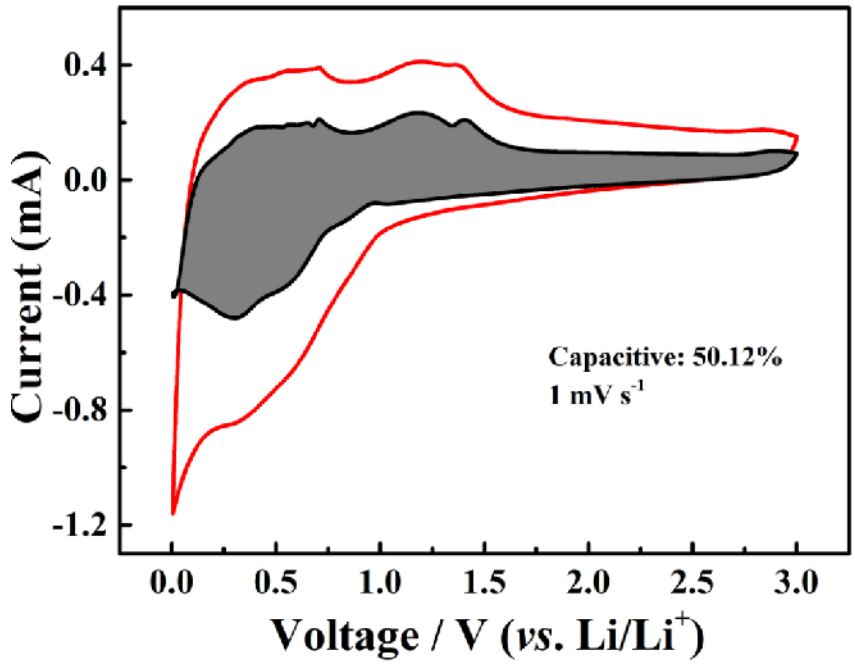

Supplementary Figure 11. Separation of the capacitive current in the ZnS/PCFs anode at a scan rate of 1 mV s^{-1}.

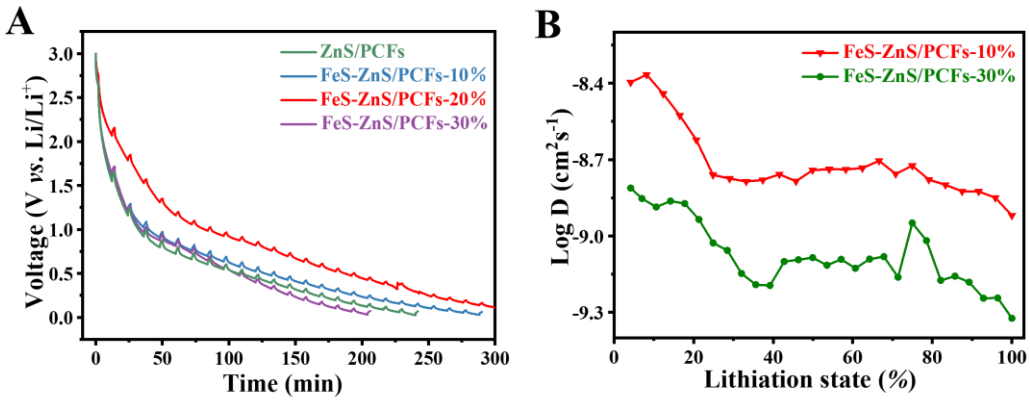

Supplementary Figure 12. A: GITT curves of the FeS-ZnS/PCFs-10% and FeS-ZnS/PCFs-30% anodes; B: Corresponding Li^+ diffusion coefficient of the FeS-ZnS/PCFs-10% and FeS-ZnS/PCFs-30% anodes.

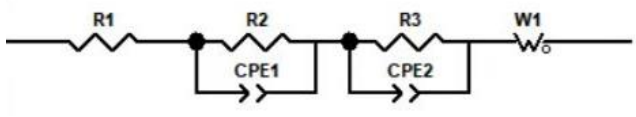

Supplementary Figure 13. Equivalent circuit of the Nyquist plot.

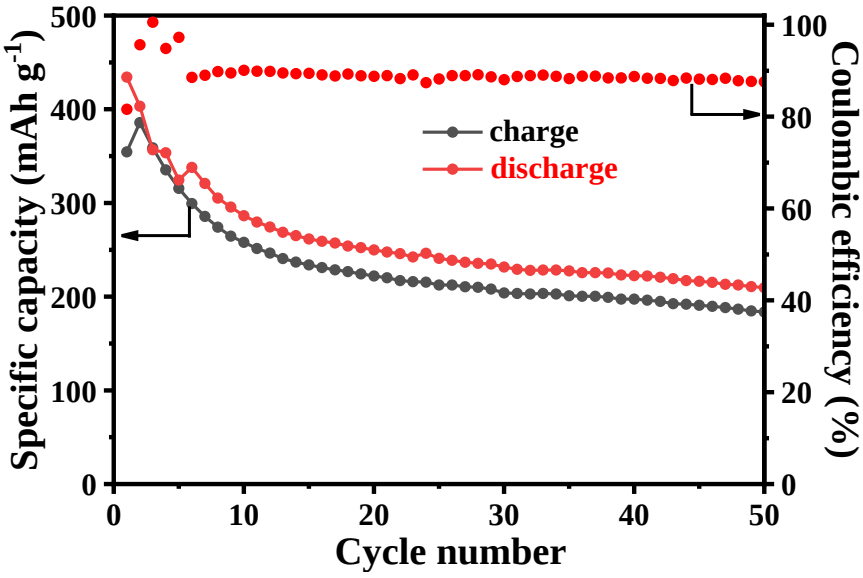

Supplementary Figure 14. Cycling performance of the FeS-ZnS/PCFs-20% //LFP full cell for 50 cycles at 0.2 A g^{-1}.

Supplementary Table 1 TEM-EDS Elemental Analysis of FeS-ZnS/PCFs-20%.

Element	Wt%	At%
C(K)	69.30	83.55
N(K)	6.80	7.03
O(K)	4.25	3.85
S(K)	4.56	2.06
Fe(K)	4.64	1.20
Zn(K)	10.45	2.31

Supplementary Table 2 Comparison of lithium storage performance of as prepared samples at different current densities.

Sample	Current density (A g^{-1})	Capacity (mAh g^{-1})
ZnS/PCFs	1	678.6
	2	582.6
	3	539.4
	4	512.5
	5	491.5
FeS-ZnS/PCFs-10%	1	953.7
	2	766.7
	3	706.4
	4	633.6
	5	603.3
FeS-ZnS/PCFs-20%	***1***	***928***
	2	***832.6***
	3	***800.7***
	4	***780***
	5	***764.2***
FeS-ZnS/PCFs-30%	1	795.4
	2	758.7
	3	727.5
	4	701.3
	5	699.3